

A Unified Attention U-Net Framework for Cross-Modality Tumor Segmentation in MRI and CT

Nishan Rai^{*1} and Pushpa R. Dahal²

¹Department of Computer Science, New Mexico State University

²Department of Plant and Environmental Sciences, New Mexico State University

2025

Abstract

This study presents a unified Attention U-Net architecture trained jointly on MRI (BraTS 2021) and CT (LIDC-IDRI) datasets to investigate the generalizability of a single model across diverse imaging modalities and anatomical sites. Our proposed pipeline incorporates modality-harmonized preprocessing, attention-gated skip connections, and a modality-aware Focal Tversky loss function. To the best of our knowledge, this study is among the first to evaluate a single Attention U-Net trained simultaneously on separate MRI (BraTS) and CT (LIDC-IDRI) tumor datasets, without relying on modality-specific encoders or domain adaptation. The unified model demonstrates competitive performance in terms of Dice coefficient, IoU, and AUC on both domains, thereby establishing a robust and reproducible baseline for future research in cross-modality tumor segmentation.

Keywords: Attention U-Net, Cross-Modality Segmentation, MRI, CT, Tumor Segmentation, Cross-modality Learning, Focal Tversky Loss

1 Introduction

Deep convolutional encoder-decoder networks such as U-Net [1] are the de facto standard for medical image segmentation. Extensions incorporating attention mechanisms [2] and loss functions tailored to class imbalance [3, 4] have further improved small-lesion sensitivity. Despite these advancements, the prevailing literature predominantly focuses on single-modality and single-organ paradigms, whereas clinical practice routinely involves heterogeneous modalities (e.g., MRI for brain and CT for lung imaging). This observation prompts a critical inquiry: can a single model, trained jointly across modalities and anatomies, learn generalized features without the need for modality-specific encoders or domain adaptation? We investigate this question by training a single Attention U-Net on two widely used datasets: BraTS 2021 brain MRI [5] and LIDC-IDRI lung CT [6]. While cross-modality domain adaptation is well-studied (e.g., SIFA [7], Dou *et al.* [8]), our emphasis is orthogonal: rather than adapt one trained model to a new modality, we examine whether a *unified* model trained simultaneously on heterogeneous data can serve as a simple, resource-friendly baseline. Our contributions are as follows: (1) the first unified Attention U-Net jointly trained across MRI (BraTS) and CT (LIDC) tumor datasets; (2) a modality-harmonized training strategy employing attention-gated skip connections and Focal Tversky loss; and (3) extensive experiments demonstrating that a single model can generalize across heterogeneous imaging domains, thereby establishing a robust baseline for future cross-modality segmentation research.

^{*}Correspondence to: nishan173@gmail.com

2 Related Work

U-Net and its Variants. Convolutional encoder-decoder networks have become the backbone of biomedical segmentation since the introduction of U-Net [1]. Building upon this, numerous variants have been proposed to improve robustness and adaptability. nnU-Net [9] introduced a self-configuring framework that adapts preprocessing, architecture, and training automatically to a given dataset. Nested architectures such as UNet++ [10] refine skip connections with dense convolutional blocks to capture multi-scale features. More recently, hybrid architectures combining convolution and transformers, including TransUNet [11] and Swin-UNet [12], have demonstrated superior performance on large-scale medical benchmarks by leveraging long-range dependencies.

Losses for Class Imbalance. Lesion segmentation is challenging due to the high class imbalance between small tumor regions and the background. While Dice loss is commonly used, Salehi *et al.* [3] introduced the Tversky loss as a generalization to control false positives and false negatives. Abraham and Khan [4] extended this with the Focal Tversky loss to emphasize harder-to-segment regions. Other alternatives include boundary-aware losses such as Boundary Loss [13] and set-based objectives like the Lovász-Softmax loss [14], both of which aim to better align optimization with evaluation metrics such as IoU.

Multi-Modal Segmentation. Medical imaging often requires leveraging complementary information across modalities. Early approaches such as HeMIS [15] and Hetero-Modal learning [16] explored fusing available modalities in a modality-invariant latent space, enabling flexible inference when some channels are missing. Valindria *et al.* [17] investigated unpaired multi-modal learning across CT and MRI for multi-organ segmentation, while Zhou *et al.* [18] proposed 3D multi-organ segmentation frameworks that exploit multi-modal cues.

Cross-Modality Domain Adaptation. Another line of work focuses on mitigating domain shift between modalities by learning modality-invariant features. Dou *et al.* [8] introduced adversarial learning for cross-modality segmentation. Chen *et al.* [7] proposed SIFA, a synergistic framework combining image-level and feature-level adaptation between MRI and CT. Similarly, Huo *et al.* [19] developed SynSegNet, which leverages synthetic images to bridge modality gaps. While these methods show strong results, they often require complex training pipelines and modality translation components.

Our Contribution. In contrast to these resource-intensive strategies, this work investigates whether a single, unified model trained jointly on mixed batches of MRI and CT data can achieve robust segmentation performance. Unlike prior studies that design separate modality-specific encoders or rely on complex domain adaptation schemes, our approach prioritizes simplicity. To the best of our knowledge, this represents the first attempt to train a unified model across heterogeneous MRI and CT tumor datasets, providing a straightforward yet effective baseline for future research in cross-modality tumor segmentation.

3 Datasets

BraTS 2021 (MRI). We utilized the RSNA-ASNR-MICCAI BraTS 2021 challenge dataset [5], comprising pre-operative multi-parametric MRI scans (T1, T1ce, T2, FLAIR) illustrated in Figure 1a. These modalities provide complementary soft tissue contrasts that facilitate accurate tumor delineation.

LIDC-IDRI (CT). We employed the LIDC-IDRI thoracic CT database [6], consisting of lung CT scans annotated by four radiologists. Consensus masks were derived via majority voting to ensure the reliability of the tumor annotations (Figure 1b).

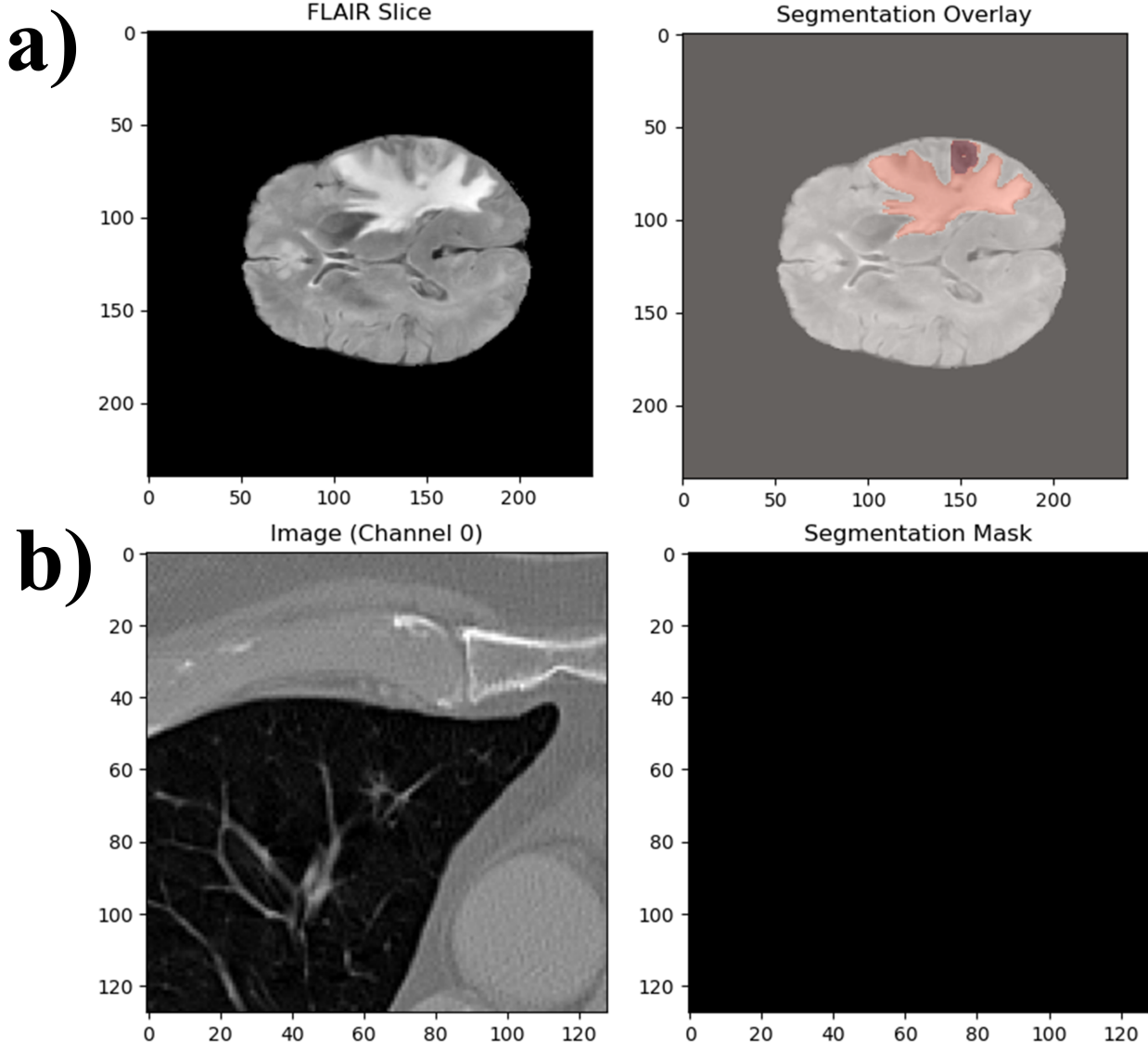


Figure 1: Representative slices from the datasets utilized in this study a. BraTS 2021 MRI slice (FLAIR modality) with an overlaid tumor mask. b. LIDC-IDRI CT slice displaying the lung nodule segmentation mask.

4 Methods

4.1 Preprocessing and Augmentation

To ensure consistent input dimensions across datasets, all axial slices were resized to 128×128 pixels. Intensity values were linearly normalized to the range $[0, 1]$ on a per-slice basis. For the BraTS dataset, MRI volumes were sliced axially, and the four modalities (T1, T1ce, T2, FLAIR) were stacked to form 4-channel input tensors [5]. In the case of the LIDC-IDRI CT slices [6], which are natively grayscale, channel replication was employed to generate 4-channel tensors, ensuring architectural consistency with the MRI inputs.

To improve model generalization and robustness, we applied a comprehensive suite of geometric and photometric augmentations via the Albumentations library [20]. These included random horizontal and vertical flips, arbitrary rotations ($\pm 15^\circ$), elastic deformations, brightness and contrast adjustments, and coarse dropout (grid masking). This augmentation strategy was applied on-the-fly during the training phase to simulate varied anatomical and acquisition conditions.

4.2 Network Architecture

We adopt the Attention U-Net architecture [2], which enhances the standard U-Net backbone [1] by integrating attention gates into the skip connections. This mechanism allows the model to selectively suppress irrelevant encoder features while highlighting salient regions in the decoder, thereby improving segmentation accuracy for irregular tumor boundaries.

Backbone Structure. The network follows a symmetric encoder–decoder design. The encoder consists of two stages that progressively compress spatial resolution while expanding feature depth (channels: $4 \rightarrow 64 \rightarrow 128$). A bottleneck layer further expands the representation to 256 channels and applies dropout ($p = 0.3$) for regularization. The decoder reconstructs spatial detail through two upsampling stages (channels: $256 \rightarrow 128 \rightarrow 64$). Skip connections bridge corresponding encoder and decoder layers at matching scales to preserve high-frequency spatial information.

Attention Gates. At each skip connection, an attention gate filters encoder features x based on a gating signal g derived from the decoder. The attention coefficients are computed as:

$$\alpha = \sigma(\psi^T (W_x x + W_g g + b)), \quad (1)$$

where W_x and W_g are 1×1 convolutions, b is a bias term, and σ denotes the sigmoid activation. The modulated output is obtained via element-wise multiplication:

$$x' = \alpha \cdot x, \quad (2)$$

which suppresses background responses while propagating tumor-relevant features forward.

Segmentation Head. A final 1×1 convolution maps decoder features to a single-channel probability map, followed by a sigmoid activation to produce the binary segmentation mask. The full network comprises approximately 1.89 million trainable parameters and requires ~ 7.3 G multiply–add operations, providing a lightweight yet expressive backbone suitable for joint MRI+CT training. Architectural details are illustrated in Fig. 2.

4.3 Loss Function and Optimization

To address class imbalance between tumor and background pixels, we employ the Focal Tversky Loss [4]. This loss extends the Tversky Index by introducing a focal parameter that down-weights easily classified examples, encouraging the model to focus on hard-to-segment regions.

Let $p_i \in [0, 1]$ denote the predicted probability for pixel i , and let $g_i \in \{0, 1\}$ denote the corresponding ground-truth label. The Tversky Index (TI) is defined as:

$$TI(p, g) = \frac{\sum_i p_i g_i}{\sum_i p_i g_i + \alpha \sum_i (1 - p_i) g_i + \beta \sum_i p_i (1 - g_i)}, \quad (3)$$

where α and β control the penalties for false negatives and false positives, respectively. Modality-specific values of (α, β) are used to account for the differing characteristics of MRI and CT datasets.

The corresponding Tversky loss is:

$$\mathcal{L}_{\text{Tversky}} = 1 - TI(p, g). \quad (4)$$

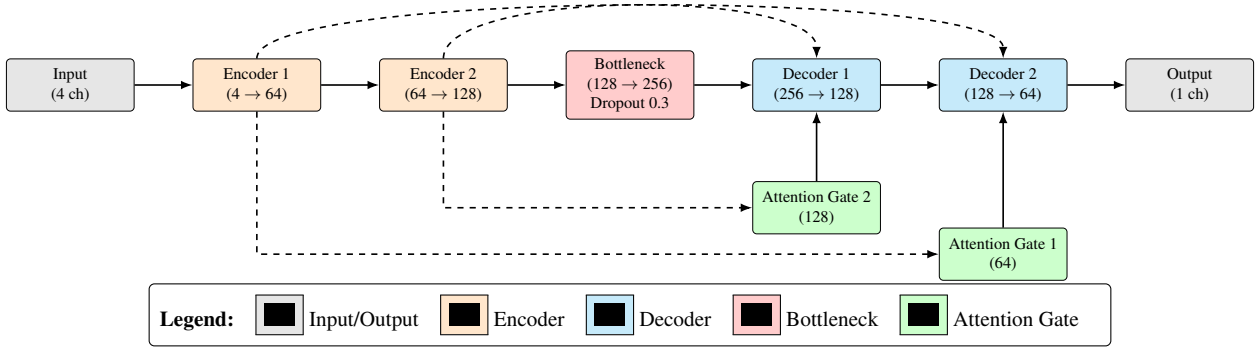


Figure 2: Architectural schematic of the proposed Attention U-Net model. The Input/Output blocks (gray) define the data ingestion and final segmentation layers. The Encoder (orange) functions as the contracting path, compressing spatial dimensions to extract hierarchical features. The Bottleneck (red) captures high-level semantic representations, incorporating dropout for regularization. The Decoder (blue) serves as an expanding path, upsampling feature maps to reconstruct the segmentation mask. Attention Gates (green) selectively filter encoder feature maps prior to concatenation to suppress irrelevant activations, while Skip Connections (dashed lines) preserve critical spatial details.

To further emphasize hard examples, the Focal Tversky loss introduces a focusing parameter γ :

$$\mathcal{L}_{\text{FTL}} = (1 - \text{TI}(p, g))^\gamma, \quad (5)$$

which increases the contribution of misclassified pixels to the total loss.

Network parameters are optimized using the AdamW optimizer [21]. To accelerate convergence, we adopt the 1-cycle learning rate policy [22], which linearly increases the learning rate to a maximum value and subsequently decreases it during the remainder of training. All experiments are implemented in PyTorch [23].

4.4 Unified Training Strategy

We adopt a single Attention U-Net that is shared across both imaging modalities, without modality-specific encoders or task-specific output heads. To encourage stable convergence on CT, we first pretrain the network for 5 epochs on LIDC-IDRI alone using the focal Tversky loss with $(\alpha, \beta) = (0.5, 0.5)$. The resulting weights are then used to initialize the unified model.

Subsequently, we fine-tune the network jointly on BraTS and LIDC-IDRI using balanced minibatches. Each training batch is constructed to contain an equal number of slices from each dataset (a 1:1 ratio), so that the optimizer receives comparable signal from MRI and CT domains. We optimize the model with AdamW (learning rate 1×10^{-4} , weight decay 1×10^{-5}) and a one-cycle learning rate policy, and we train with a batch size of 8.

Validation is performed separately on held-out BraTS and LIDC-IDRI splits. At each epoch, we compute validation Dice and loss per modality and select the best checkpoint based on the macro-averaged Dice across MRI and CT to avoid overfitting to a single domain.

5 Experiments

5.1 Evaluation Protocol

Segmentation performance is assessed using standard metrics, including the Dice Similarity Coefficient (Dice), Intersection over Union (IoU), Precision, Recall, F1-score, and the Area Under the Receiver Operating Characteristic Curve (ROC-AUC). These metrics provide a comprehensive evaluation of model accuracy, boundary adherence, and classification confidence. The ROC-AUC is computed by varying the probability threshold and measuring the area under the resulting curve.

Let p denote the predicted binary segmentation mask and g the corresponding ground-truth mask. True positives (TP), false positives (FP), true negatives (TN), and false negatives (FN) are computed on a pixel-wise basis.

$$\text{Dice}(p, g) = \frac{2|p \cap g|}{|p| + |g|}, \quad (6)$$

$$\text{IoU}(p, g) = \frac{|p \cap g|}{|p \cup g|}, \quad (7)$$

$$\text{Precision} = \frac{TP}{TP + FP}, \quad \text{Recall} = \frac{TP}{TP + FN}, \quad (8)$$

$$F1 = \frac{2 \cdot \text{Precision} \cdot \text{Recall}}{\text{Precision} + \text{Recall}}. \quad (9)$$

5.2 Quantitative Results

Table 1 summarizes the test performance of the unified model across the BraTS and LIDC-IDRI datasets. The model demonstrates stronger performance on MRI (BraTS), achieving a Dice score of 0.83 and an AUC of 0.97. In contrast, performance on CT (LIDC-IDRI) is comparatively lower, yielding a Dice score of 0.55 and an AUC of 0.83. The aggregated “unified” performance reflects a compromise between these domains, with a Dice of 0.64 and an AUC of 0.90.

Table 1: Test performance metrics by dataset (unified model).

Dataset	Dice	IoU	Precision	Recall	F1	AUC
BraTS	0.83	0.80	0.86	0.92	0.84	0.97
LIDC	0.55	0.49	0.74	0.69	0.57	0.83
Unified	0.64	0.59	0.78	0.77	0.66	0.90

5.3 Training Dynamics

The training and validation trajectories for loss and Dice score are depicted in Figure 3. A rapid decline in training and validation loss is observed for the BraTS dataset, accompanied by a corresponding increase in the Dice score, which reaches approximately 0.8 by epoch 5. Conversely, the LIDC validation loss exhibits higher volatility and remains elevated throughout training, consistent with the challenges posed by smaller lesion sizes and higher noise levels in CT data. Despite this, the Dice score for LIDC shows gradual improvement, stabilizing around 0.55. These dynamics indicate that while the unified architecture generalizes effectively to MRI segmentation, the task remains more complex for CT data.

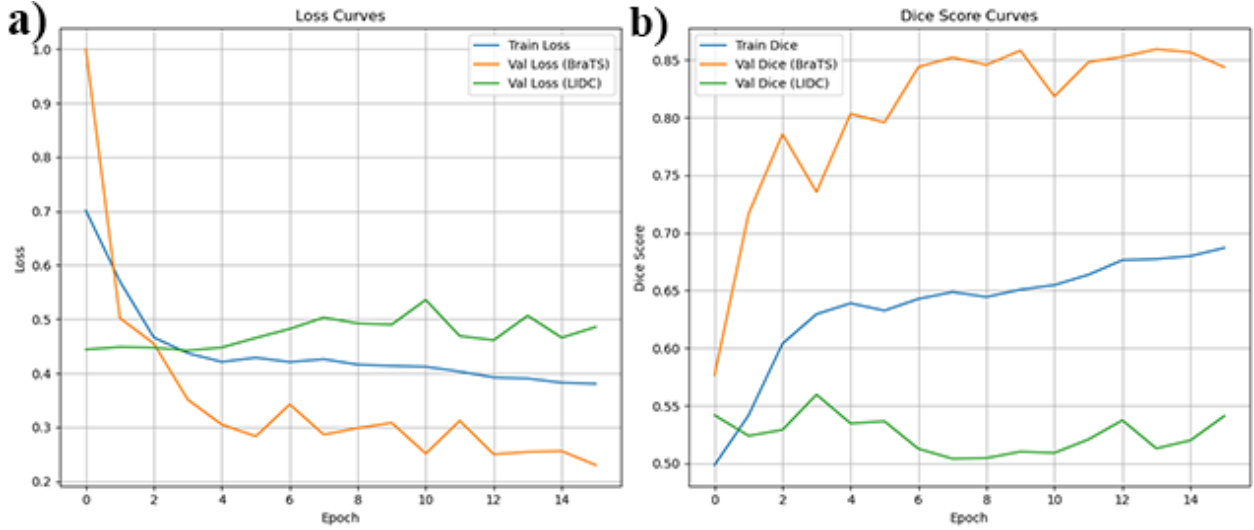


Figure 3: Training and validation curves showing a. loss and b. Dice score across epochs for both MRI (BraTS) and CT (LIDC-IDRI).

5.4 ROC and Confusion Analysis

To further analyze decision thresholds, Fig. 4 shows the unified ROC curve with an AUC of 0.89, indicating reliable discrimination despite a lower Dice score. The confusion matrices (Fig. 4) illustrate that false negatives dominate CT predictions, whereas MRI predictions achieve stronger recall with fewer misclassifications.

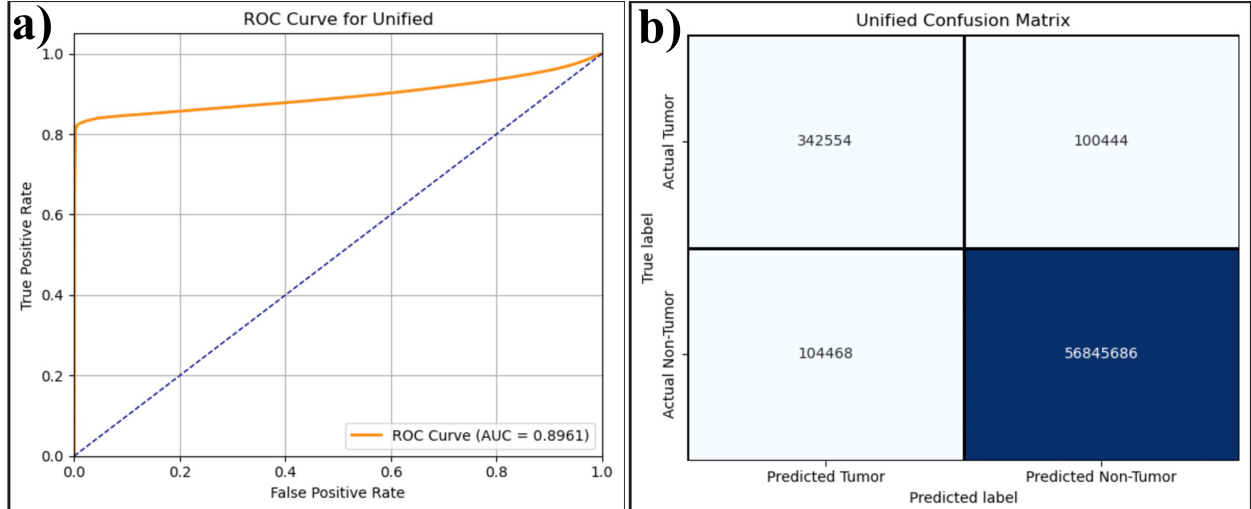


Figure 4: Performance analysis of the unified Attention U-Net framework on both datasets. (a) Unified ROC curve for test set (AUC = 0.89). (b) Unified confusion matrix.

5.5 Qualitative Results

Representative segmentation results for MRI and CT slices are displayed in Figure 5. Visual inspection confirms that the model accurately captures tumor boundaries in MRI images. However, for CT images,

predictions occasionally under-segment small nodules, corroborating the quantitative findings regarding the difficulty of detecting smaller lesions in the LIDC-IDRI dataset.

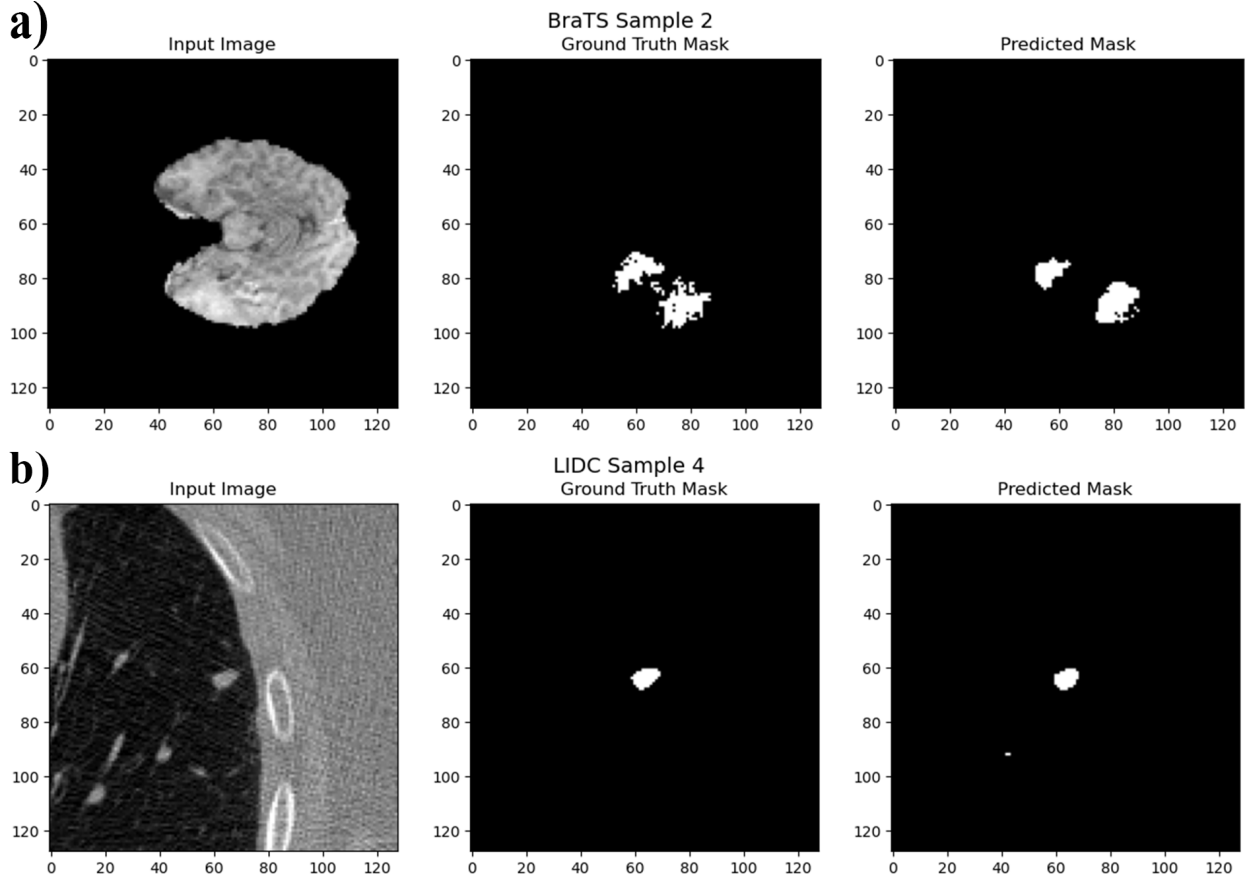


Figure 5: Qualitative segmentation results for the unified model. The top panel a. displays results for BraTS Sample 2, and the bottom panel b. for LIDC Sample 4. Each sample row presents the input image, ground truth mask, and predicted mask to visualize segmentation performance on MRI and CT modalities.

6 Discussion

The unified Attention U-Net balances performance across different imaging modalities, achieving high recall on MRI (BraTS) and solid precision on CT (LIDC-IDRI). The attention mechanism appears particularly effective at capturing diffuse, irregular MRI tumor boundaries, reducing the risk of missed detections, while still identifying high-density CT nodules with reasonable accuracy.

Qualitatively, the model adapts well without modality-specific tuning. In BraTS Sample 2 (Fig. 5a), predictions align closely with complex tumor boundaries and edema, despite substantial variation in MRI intensity. Similarly, in LIDC Sample 4 (Fig. 5b), the model successfully segments a lung nodule embedded within heterogeneous thoracic tissue. These observations suggest that attention gates help suppress irrelevant structures, such as skull artifacts or ribs—while prioritizing pathology-relevant features.

Compared to domain-adaptation approaches that rely on adversarial training or image translation, the proposed unified framework is considerably simpler to train and deploy. However, the substantial intensity and contrast shift between MRI and CT remains a key challenge. Future work may explore modality-aware

adapter layers or lightweight domain-conditioning mechanisms to improve CT precision without sacrificing architectural simplicity.

7 Limitations and Societal Impact

This study uses a single-GPU workstation and does not include extensive hyperparameter sweeps, which likely leaves some performance improvements unexplored. Additionally, treating 3D volumes as independent 2D slices misses critical spatial context needed for accurate volume assessment. Future work should explore volumetric (3D) architectures to address this. Translating this model to the clinic requires responsibility. While robust on benchmarks, rigorous validation is needed to ensure it handles diverse populations and scanner types. Performance drops are possible in unseen real-world scenarios. Segmentation errors could delay diagnosis, so this system must remain a decision-support tool rather than an autonomous diagnostician. It should serve as a "second opinion" for radiologists. Ensuring robustness against artifacts and maintaining human oversight is essential before hospital deployment.

8 Conclusion

A unified Attention U-Net framework was presented for cross-modality tumor segmentation, targeting the heterogeneous domains of brain MRI and thoracic CT. Through extensive experimentation on BraTS 2021 and LIDC-IDRI datasets, it was demonstrated that a single architecture, bolstered by attention mechanisms, can generalize across distinct modalities without the need for domain adaptation modules like adversarial training. The qualitative and quantitative results establish a novel, reproducible baseline for future research on cross-domain and multi-modal segmentation. This work highlights the potential of simplified, attention-based architectures to reduce the engineering burden associated with maintaining separate models for different imaging modalities.

9 Acknowledgements

This manuscript resulted from the final class project work of APPLIED ML I (CS 519). The authors would like to thank the Computer Science Department at New Mexico State University for providing facilities and technical support. Furthermore, the authors acknowledge Assistant Prof. Tuan Le for the opportunity to conduct this research and for his guidance throughout the project.

Reproducibility and Code Availability To facilitate reproducibility, all preprocessing scripts, training schedules, random seeds, and configuration defaults have been released publicly via our project repository: <https://github.com/Nishan8912/unified-attention-unet-cross-modality>.

References

- [1] Olaf Ronneberger, Philipp Fischer, and Thomas Brox. U-net: Convolutional networks for biomedical image segmentation. In *MICCAI*. Springer, 2015. doi: 10.1007/978-3-319-24574-4_28. URL <https://arxiv.org/abs/1505.04597>.
- [2] Ozan Oktay, Jo Schlemper, Loic Le Folgoc, et al. Attention u-net: Learning where to look for the pancreas. *arXiv preprint arXiv:1804.03999*, 2018. URL <https://arxiv.org/abs/1804.03999>.

- [3] S. S. M. Salehi, Deniz Erdogmus, and Ali Gholipour. Tversky loss function for image segmentation using 3d fully convolutional deep networks. *arXiv preprint arXiv:1706.05721*, 2017. URL <https://arxiv.org/abs/1706.05721>.
- [4] Nabila Abraham and Naimul Mefraz Khan. A novel focal tversky loss function with improved attention u-net for lesion segmentation. In *IEEE ISBI*, 2019. URL <https://arxiv.org/abs/1810.07842>. arXiv:1810.07842.
- [5] Ujjwal Baid, Snehalata Ghodasara, Michel Bilello, et al. The rsna-asnr-miccai brats 2021 benchmark. *arXiv preprint arXiv:2107.02314*, 2021. URL <https://arxiv.org/abs/2107.02314>.
- [6] Samuel G Armato, Geoffrey McLennan, Luc Bidaut, et al. The lung image database consortium (lidc) and image database resource initiative (idri): A completed reference database of lung nodules on ct scans. *Medical Physics*, 38(2):915–931, 2011. doi: 10.1118/1.3528204. URL <https://pubmed.ncbi.nlm.nih.gov/21452728/>.
- [7] Cheng Chen, Qi Dou, Hao Chen, Jing Qin, and Pheng-Ann Heng. Unsupervised bidirectional cross-modality adaptation via deeply synergistic image and feature alignment for medical image segmentation. *IEEE Transactions on Medical Imaging*, 39(7):2494–2505, 2020. doi: 10.1109/TMI.2020.2968894. URL <https://arxiv.org/abs/1901.08211>.
- [8] Qi Dou, Cheng Ouyang, Cheng Chen, Hao Chen, and Pheng-Ann Heng. Unsupervised cross-modality domain adaptation of convnets for biomedical image segmentations with adversarial loss. *arXiv preprint arXiv:1804.10916*, 2018. URL <https://arxiv.org/abs/1804.10916>.
- [9] Fabian Isensee et al. nnu-net: a self-configuring method for deep learning-based biomedical image segmentation. *Nature Methods*, 18(2):203–211, 2021. doi: 10.1038/s41592-020-01008-z. URL <https://www.nature.com/articles/s41592-020-01008-z>.
- [10] Zongwei Zhou, Md Mahfuzur Rahman Siddiquee, Nima Tajbakhsh, and Jianming Liang. Unet++: A nested u-net architecture for medical image segmentation. In *DLMIA*, 2018. URL <https://arxiv.org/abs/1807.10165>.
- [11] Jieneng Chen, Yongyi Lu, Qihang Yu, et al. Transunet: Transformers make strong encoders for medical image segmentation. In *MICCAI*, 2021. URL <https://arxiv.org/abs/2102.04306>.
- [12] Hu Cao, Yue Wang, Joy Chen, Dong Jiang, Xiang Zhang, Qi Tian, and Mao Wang. Swin-unet: Unet-like pure transformer for medical image segmentation. *arXiv preprint arXiv:2105.05537*, 2021.
- [13] Hoel Kervadec, J. Bouchtiba, C. Desrosiers, et al. Boundary loss for highly unbalanced segmentation. In *MICCAI*, 2019. URL <https://arxiv.org/abs/1812.07032>.
- [14] Maxim Berman, Amal Triki, and Matthew B. Blaschko. The lovasz-softmax loss: A tractable surrogate for the optimization of the intersection-over-union measure in neural networks. In *CVPR*, 2018. URL <https://arxiv.org/abs/1705.08790>.
- [15] Mohammad Havaei, Nicolas Guizard, Nicolas Chapados, and Yoshua Bengio. Hemis: Hetero-modal image segmentation. *International Conference on Medical Image Computing and Computer-Assisted Intervention*, 2016.
- [16] Agisilaos Chartsias, Thomas Joyce, Mario Valerio Giuffrida, and Sotirios A. Tsaftaris. Multimodal mr synthesis via modality-invariant latent representation. In *IPMI*, 2017. URL <https://arxiv.org/abs/1704.07747>.

- [17] Vanya V. Valindria, Kamlesh Pawar, Martin Rajchl, et al. Multi-modal learning from unpaired images: Application to multi-organ segmentation in ct and mri. In *WACV*, 2018. URL <https://arxiv.org/abs/1804.07587>.
- [18] Zongwei Zhou, Vibha Sodha, Md Mahfuzur Rahman Siddiquee, Ruibin Feng, Nima Tajbakhsh, Michael B Gotway, and Jianming Liang. Models genesis: Generic autodidactic models for 3d medical image analysis. In *Medical Image Computing and Computer Assisted Intervention (MICCAI)*, pages 384–393. Springer, 2019.
- [19] Yuankai Huo, Zhoubing Xu, Shunxing Bao, Albert Assad, Richard Abramson, and Bennett Landman. Synseg-net: Synthetic segmentation without target modality ground truth. In *ISBI*, 2018. URL <https://arxiv.org/abs/1806.02758>.
- [20] Alexander Buslaev, Vladimir I. Iglovikov, Eugene Khvedchenya, et al. Albumentations: Fast and flexible image augmentations. *Information*, 11(2):125, 2020. doi: 10.3390/info11020125. URL <https://www.mdpi.com/2078-2489/11/2/125>.
- [21] Ilya Loshchilov and Frank Hutter. Decoupled weight decay regularization. In *ICLR*, 2019. URL <https://openreview.net/forum?id=Bkg6RiCqY7>.
- [22] Leslie N. Smith and Nicholay Topin. Super-convergence: Very fast training of neural networks using large learning rates. *arXiv preprint arXiv:1708.07120*, 2018. URL <https://arxiv.org/abs/1708.07120>.
- [23] Adam Paszke, Sam Gross, Francisco Massa, et al. Pytorch: An imperative style, high-performance deep learning library. In *NeurIPS*, 2019. URL <https://arxiv.org/abs/1912.01703>.